CrossMark

Microstructure and Corrosion Behavior of Thermal-Sprayed Hydroxyapatite/Magnesium Composite Coating on the Surface of AZ91D Magnesium Alloy

Hai-Long Yao[1] · Xiao-Zhen Hu[2] · Hong-Tao Wang[1] · Qing-Yu Chen[1] ·
Xiao-Bo Bai[1] · Meng-Xian Zhang[1] · Gang-Chang Ji[1]

Abstract To slow down the corrosion rate and increase the bioactivity of magnesium alloys, biodegradable hydroxyapatite/magnesium (HA/Mg) composite coating was deposited onto AZ91D alloy substrate by high-velocity suspension flame spray technique using nano-sized HA and micron-sized Mg powders. Microstructures and phase constitutions of HA/Mg composite coating were analyzed by scanning electron microscopy and x-ray diffraction. Corrosion resistance of composite coating was also evaluated by potentiodynamic polarization test and electrochemical impedance spectroscopy in Hanks' balanced salt solution (HBSS). The result shows that the HA/Mg composite coating mainly consisted of Mg and HA in addition to a few of MgO phases. The coating showed a rough surface morphology with homogeneous elemental distribution and a lamellar structure in cross section as well as well-bonded coating/substrate interface. Mg particles presented superior deposition during spraying due to their higher melting degree compared to HA particles. AZ91D alloy substrate was significantly protected from corrosion in HBSS by the HA/Mg composite coating with Mg dissolution on surfaces of the composite coating. This strategy can offer a new route to fabricate HA/Mg composite coatings on other metal substrates for use in biodegradable implant fields.

Keywords AZ91D alloy · corrosion resistance · HA/Mg composite coating · HVSFS · microstructure

Introduction

The well biodegradability in the physiological body environment and the similar mechanical properties to human bone of magnesium (Mg) alloys has made them to be potential for implant materials over other metallic materials (Ref 1), such as Ti and Fe. However, Mg alloy implants cannot provide effective biomechanical support and promote bone reconstruction because of their rapid corrosion rates and low bioactivities (Ref 1, 2). Therefore, there is a challenge to improve the corrosion resistance and bioactivity of Mg alloys for actual applications.

To slow down the corrosion rate and enhance the bioactivity of Mg alloys, preparation of coatings on the substrate surfaces is a potential method (Ref 1-4). These coatings not only protect the substrate from corrosion, but also improve the bioactivities of Mg alloy substrates. Up to now, many materials have been coated on the surface of Mg alloys, such as CeO_2 (Ref 5), stearic acid (Ref 6), polymeric (Ref 7), Nb_2O_5 (Ref 8), ZrO_2 (Ref 9) and so on. Among those materials, hydroxyapatite (HA) has a similar chemical composition to human bone (Ref 2, 10), which is widely used as coatings on the surfaces of Mg alloys. However, HA has poor mechanical properties with the brittle nature and puts forward a significant difference of thermal expansion coefficient from Mg alloys (Ref 1-4). Those phenomenon result in cracking between the HA coating and Mg alloy substrates. To increase the

✉ Gang-Chang Ji
jigangchang@126.com

Hai-Long Yao
yhl206@163.com

1 Jiangxi Province Engineering Research Center of Materials Surface Enhancing and Remanufacturing, School of Mechanical and Materials Engineering, Jiujiang University, Jiujiang 332005, China

2 School of Civil Engineering and City Construction, Jiujiang University, Jiujiang 332005, China

mechanical properties of HA coatings, different reinforcements have been added into the HA coatings to form HA-based composite coatings, such as ceramics (Ref 11), metal (Ref 12) and polymers (Ref 13, 14). Following consideration of the requirement of biodegradability for the substrates and coatings, the reinforcements used in the HA coatings and the substrates should be biodegradable (Ref 15-18). Due to the biodegradability of the Mg metal, HA/Mg composite is considered as one of the potential coatings onto the Mg substrate. Recently, HA/Mg composite coatings have been developed for implant applications using low-temperature methods such as electromagnetic induction deposition (Ref 19) and chemical conversion deposition (Ref 16). High-velocity suspension flame spray (HVSFS) technique is another coating deposition technology, which has been widely used to deposit HA or HA-based coatings onto different metals or alloys substrates owing to the high-deposition efficiency (Ref 20-22). However, because of easy combustion of Mg particles, the preparation of HA/Mg composite coating by thermal spraying technique has not been reported.

The purpose of this study was to develop a HA/Mg composite coating on the surface of AZ91D alloy using HVSFS technique. Nano-sized HA and micron-sized Mg powders were used as raw materials to prepare the HA/Mg composite coating. Phase composition, microstructure and corrosion resistance of the HA/Mg composite coating were investigated.

Experimental Procedures

Materials and Suspension

To prepare the HA/Mg composite coating, both nano-sized HA powders with diameter of 20 nm and spherical micron-sized Mg powders with an average diameter of 10 μm were used as raw materials to prepare the particle suspension (Fig. 1). For preliminary study, 30 wt.% Mg powders were added into the HA powders to produce a HA/Mg particle mixture. An optimal particle suspension was prepared by using our previous method (Ref 21, 22). A 5 wt.% HA/Mg particle mixture was dispersed into 95 wt.% mixed solution. The mixed solution consisted of the distilled water and ethanol (50:50, v/v). AZ91D magnesium alloy plates with dimensions of 30 × 20 × 6 mm were used as substrates. Before coating deposition, AZ91D substrates were sand-blasted for 5 min by corundum particles of 200 μm in diameter with an air pressure of 0.4 MPa, and then ultrasonically cleaned in fresh ethanol bath for 10 min.
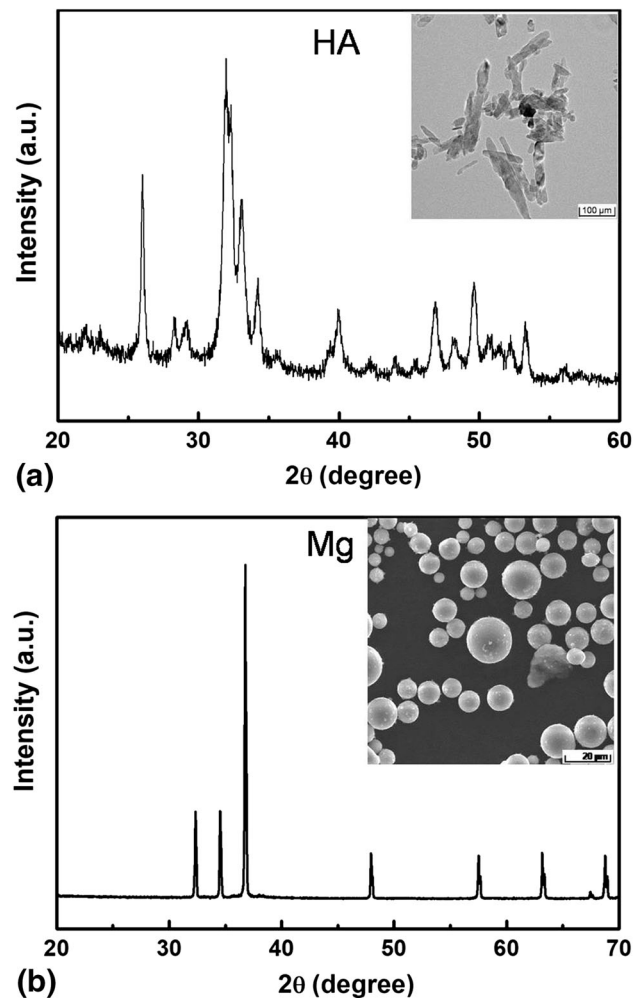

Fig. 1 Morphologies and XRD patterns of HA and Mg powders. (a) HA powder, (b) Mg powder

Table 1 HVSFS deposition parameters

Fuel (propane) flow rate, slpm	45
Oxygen flow rate, slpm	180
Suspension flow rate, ml/min	40
Spray distance, mm	100
Torch traverse speed, mm/s	200

Coating Preparations

A homemade HVSFS system was utilized to deposit the HA/Mg composite coating onto AZ91D substrate. The procedure has been described in our previous study (Ref 21, 22). The HA/Mg particle suspension was mechanically fed into the combustion chamber of the spray torch using a peristaltic pump. The sand-blasted AZ91D substrates were preheated at around 100 °C (measured using an infrared pyrometer) in the flame without feeding the suspension.

The optimal spraying parameters are given in Table 1. Except for torch speed of 1000 mm/s, the spraying parameters applied to deposit single particles onto the polished AZ91D substrate were identical to that of spraying coating.

Coating Characterization

Surface morphology and cross-sectional microstructure of the HA/Mg composite coating was examined by a scanning electron microscopy (SEM, VEGA II, Tescan, Czech Republic). The SEM system is also equipped with an energy-dispersive spectrometry (EDS) to analyze elemental distribution of composite coatings. Phase constitutions of both the HA/Mg mixed powder and composite coating were analyzed by an x-ray diffraction (XRD, D8 Advance, Bruker, Germany). The XRD analysis was operated in the reflected model with Cu-Kα radiation and a wavelength of 1.5418 Å, an operating voltage of 35 kV, and an operating current of 35 mA. A diffracted beam monochromator was accompanied by a scan rate of $0.2°/s$ over a 2θ range of 20°-70°.

Tensile strength of as-sprayed HA/Mg coating was measured using a standard tensile test method (ASTMC-633) designed for thermal-sprayed coatings. The end surface of cylindrical sample with deposited coatings was boned on grit-blasted facings of the loading fixtures, being the same size and shape as the sample, using a special adhesive glue (E-7, Adtest, Shanghai huayi resins Co. Ltd., China) with an tensile strength of about 70 MPa. The assembly was held perpendicularly and put in an oven at 100 °C for 2 h. After the adhesive glue being cured and hardened, the assembly was loaded in the machine (ZWICK, Z050 model) at a head speed of 1 mm/min. The tensile strength was assessed by the average value of at least three sample test results.

To investigate corrosion behaviors of both HA/Mg composite coating and bare AZ91D substrate, a potentiodynamic polarization test and electrochemical impedance spectroscopy (EIS) were carried out in a commercial Hanks' balanced salt solution (HBSS, H1025, Solarbio material, China). HBSS consists of 8 g/L NaCl, 0.126 g/L $Na_2HPO_4 \cdot 12H_2O$, 0.4 g/L KCl, 0.06 g/L KH_2PO_4, 0.098 g/L $MgSO_4$, 0.14 g/L $CaCl_2$, 1 g/L D-glucose, and 0.35 g/L $NaHCO_3$. A flat three-electrode cell consisting of a working electrode (coating or bare substrate), a reference electrode (Ag/AgCl electrode) and a counter electrode (Pt grid) was utilized. The HA/Mg composite coating with surface area of 1 cm^2 was exposed to the HBSS. All the samples were immersed in HBSS for 1 h before the tests. Polarization curves were measured using an electrochemical station (IM6, Zahner, Germany). The working electrode was polarized in HBSS at a temperature of 37 ± 1 °C from

− 2 to − 0.1 V (versus SCE) at a scan rate of 1 mV/s. CorrWare software was employed to estimate the corrosion potential (E_{corr}), corrosion current (I_{corr}), corrosion resistance (R_p) and corrosion rate. EIS measurements were conducted at the open-circuit potential (OCP) with an amplitude of 10 mV. The frequency ranged from 0.01 Hz to 100 kHz, with a logarithmic sweep of ten points per decade. The recorded impedance spectra were then fitted using Z-view software. For comparison, the sand-blasted AZ91D substrate was also investigated. After the polarization tests, the microstructures and phase constitutions of all samples were examined by SEM and XRD, respectively.

Results and Discussion

Phase Constitutions of HVSFS HA/Mg Composite Coating

Figure 2 shows the XRD patterns of HA/Mg mixed powder and composite coatings. The HA/Mg composite coating mainly consisted of HA and Mg in addition to a few of MgO phase. Consistent with our previous results (Ref 21, 22), the HA was not decomposed into other additional phases such as TCP, TTCP or CaO. Moreover, no mutual reaction of HA particles with Mg particles occurred. These facts indicate that the Mg and HA particles were largely preserved in the composite coating.

It is worth note that the HA/Mg composite coating contained only very few of MgO phase, although the Mg powders were subjected to the oxygen-propane flame with the temperature of higher than 1800 °C (Ref 21). Combustion of Mg particle usually has four stages: molten,
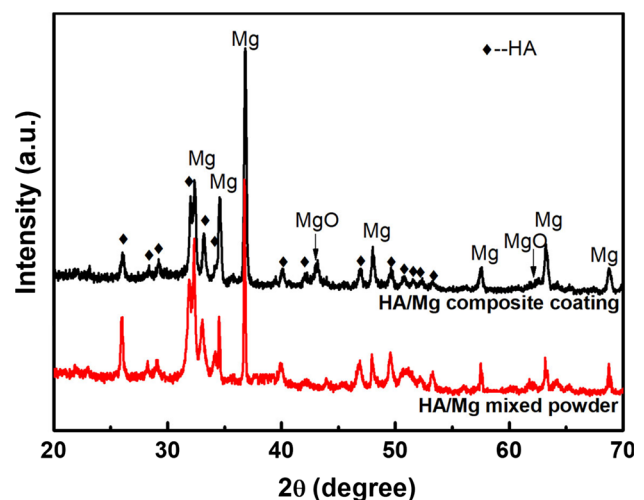

Fig. 2 XRD patterns of HA/Mg mixed powder and composite coating

expansion, inflame, and combustion (Ref 23). It is reported that the lifetime of Mg particles with 50 μm in diameter burning in the oxygen and air atmosphere is 1.30 and 1.85 ms (Ref 24), respectively. According to the mean particle velocity at the similar condition during HVSFS (Ref 21), the flying time of Mg particles from the combustion chamber of the HVSFS torch to the substrate surface was less than 1 ms. These facts indicate the limited time for Mg particle combustion during HVSFS. Furthermore, it is also reported that the combustion of Mg particles in air depends on the diffusion rate of the oxygen (Ref 24). However, the amount of residual oxygen gas was limited in the present flame after burning due to the oxygen/propane ratio of 4 with excessive propane. Figure 3 shows the typical morphology of HA/Mg splat on AZ91D substrate. The Mg particle was completely melted and flattened after impacting onto the substrate. While some agglomerates composed of nano-sized HA particles were dispersed in the melted Mg splat. It can be considered that nano-sized HA particles could adhere to the surfaces of Mg particles forming the HA shell after the solution

evaporating (see the schematic diagrams shown in Fig. 3). This Mg-core/HA-shell structure of particles can slightly hinder the heat and oxygen transferring from flame to Mg particles, which are beneficial to inhibit the oxidation of Mg particles. Therefore, a slight amount of MgO was formed on the Mg particle surface during the HVSFS.

Microstructure of HVSFS HA/Mg Composite Coating

Figure 4(a) shows that the HA/Mg composite coating presented a rough surface with different features, i.e., smooth surface splats, nanoparticle agglomerates and near-spherical droplets, which were the typical features of HA/metal composite coatings deposited by HVSFS, as described in our previous study (Ref 22). The smooth splats and near-spherical droplets are formed by melted Mg and HA particles. In contrast, the nanoparticle agglomerates with unsmooth surface are formed by the un-melt HA particles. Those surface features were consistent with the HA/Mg splats as shown in Fig. 3. EDS analysis shows that Mg, Ca,
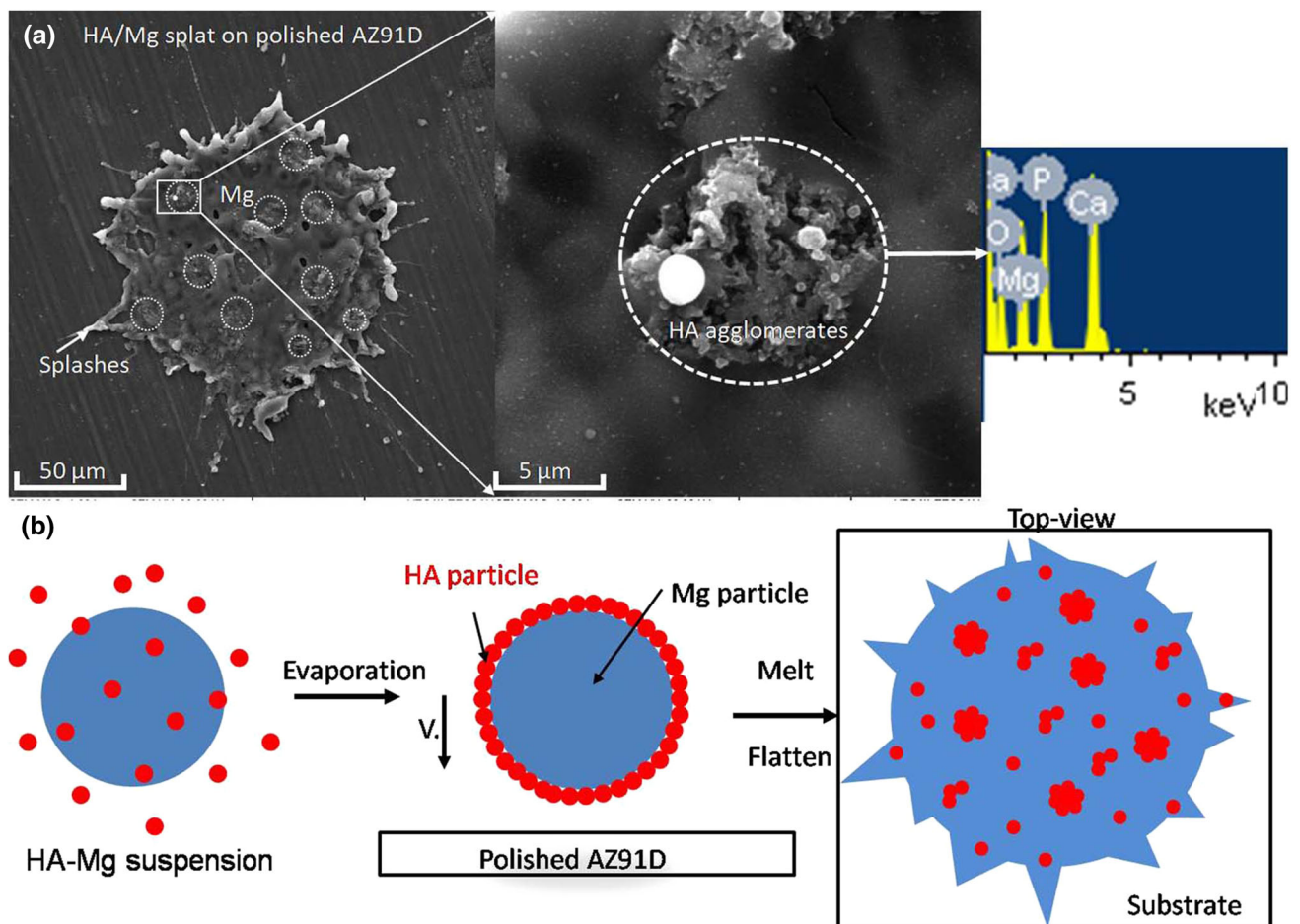

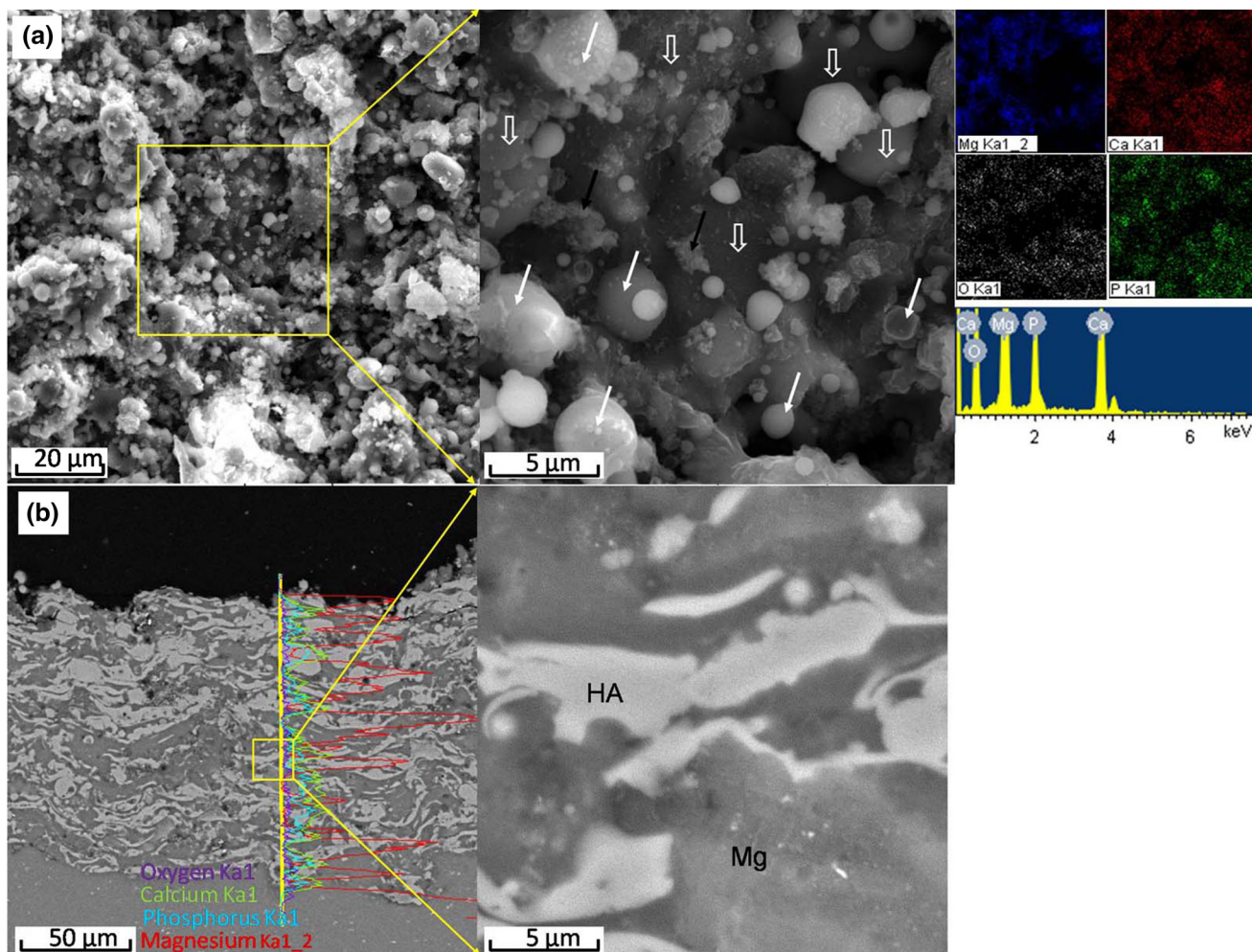**Fig. 3** SEM image (a) and schematic diagram (b) of single HA/Mg deposition

Fig. 4 Surface morphology (a) and cross-sectional microstructure (b) of HA/Mg composite coating. (In Fig. 4a, black arrows refer to nanoparticle agglomerates, white arrows refer to near-spherical splats, whit hollow arrows refer to smooth surface splats)

P, and O elements were homogeneously dispersed on the coating surface (see inset in Fig. 4a). Compared to the original Mg powder, no micron-sized spherical Mg splats were observed on the coating surface. This phenomenon indicates that the Mg particles were melted, dispersed and deformed during the coating deposition.

The cross-sectional morphology of the HA/Mg composite coating exhibits a typical lamellar structure at the BSE mode (see Fig. 4b) and exists alternatively distributed lamella with different grayscale. Moreover, the coating was well-bonded to the substrate without any obvious coating/substrate interface. According to the elemental content, the dark lamellae were rich in Mg and the gray lamellae were rich in HA. It is difficult to identify the MgO phase from the cross-sectional image due to its limited content. Conventionally, the TEC of HA is around 11-13 $\times 10^{-6}$/K (Ref 25) and the TEC of AZ91D alloy is around 28×10^{-6}/K (Ref 26). This significant difference in TEC between HA and AZ91D alloy is liable to induce cracking

in the coating during thermal spraying. However, from Fig. 4(b), there were not any obvious cracks in the HA/Mg composite coating and on coating/substrate interface. According to the tensile strength test, the bond strength of the HA/Mg composite coating was 26.7 $\pm$ 5.6 MPa. This bond strength was comparable to that of HVSFS HA/TiO$_2$ multilayer coating (Ref 21). This phenomenon can be ascribed to the match of thermal expansion coefficient (TEC) between the AZ91D substrate and HA/Mg composite coating. In addition, the HA/Mg composite coating was dense with some small isolated pores. This dense microstructure is benefit to prevent the corrosion electrolyte from penetrating into the coating/substrate interface.

By using the photo-image method, the cross section of HA/Mg composite coating consisted of 28.5 wt.% HA and 71.5 wt.% Mg. HA content in the composite coating was significantly lower than that in the starting HA/Mg mixed powder. This fact indicates the superior deposition of Mg

particles during the co-deposition of HA-Mg mixed powder. Owing to the melting points of Mg and HA are 650 °C (Ref 2) and 1570 °C (Ref 25, 27), respectively, the molten degree of Mg powder was greater than that of the HA powder HVSFS. This higher melting point of Mg particles would result in their superior depositions.

Corrosion Behavior of HVSFS HA/Mg Composite Coating

Corrosion resistance performance of Mg alloys in simulated body fluid (SBF) is usually weak (Ref 28), resulting in the rapid failure of Mg-based implants before the expected period. Preparations of coatings on Mg-based implants are the main method to improve their corrosion resistance properties (Ref 2, 10). Figure 5 shows that the HA/Mg composite coating had a lower corrosion current than the bare AZ91D substrate. Based on the potentiodynamic polarization curves, the electrochemical parameters are listed in Table 2. Compared with the bare substrate, the corrosion current of HA/Mg composite coating was decreased by ~ 7-fold from 570.5 ± 79.5 to 81.8 ± 15.2 $\mu A/cm^2$, and the corrosion resistance was increased by ~ 7-fold from 45.7 ± 12.5 to 331.9 ± 65.9 Ohms/cm^2 resulting in the decrease in corrosion rate by ~ 7-fold from 264.2 ± 56.9 to 37.4 ± 7.7 MPY. The corrosion potential was slightly decreased from -1.215 ± 0.012 to -1.482 ± 0.007 V.
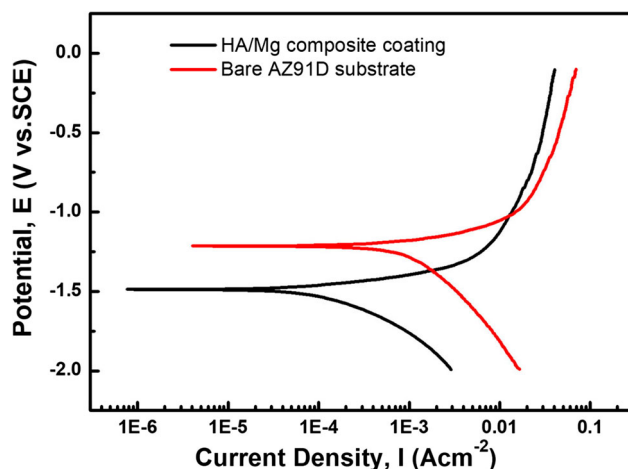
According to our previous study (Ref 22), two semicircles of the HA/Mg composite coating in EIS as shown in Fig. 6 refer to charge transfer resistance for the composite coating and coating/substrate or substrate/electrolyte interface, respectively. Thus, in the equivalent circuit (Ref 22) (see the insert in Fig. 6), R1 and CPE1 represent the charge transfer resistance and capacitive characteristics of HA/Mg composite coatings, respectively; R2 and CPE2 represent the charge transfer resistance and electrical double layer capacitance of the coating/substrate or substrate/electrolyte interface, respectively. Compared to the bare AZ91D substrate, the HA/Mg composite coating showed higher charge transfer resistance (as shown in Fig. 6 and Table 3), which was consistent with the above potentiodynamic polarization measurements. Similarly, many studies also report that HA/Mg composites or coatings on Mg substrates can show high corrosion resistances compared to the bare Mg alloys, such as HA/Mg composites (Ref 29, 30), pulsed laser-deposited HA/Mg coatings (Ref 31), and plasma-sprayed HA coatings (Ref 32). These results indicate that the HVSFS HA/Mg composite coating can also protect the AZ91D substrate against corrosion in HBSS.

Figure 7 shows the surface morphologies of both the HA/Mg composite coating and bare AZ91D substrate after the polarization tests. Compared with the as-sprayed coating, some microcracks and nanoparticles agglomerates appeared on the surface of HA/Mg composite coating (see Fig. 7a). Those microcracks resulted from the dissolution
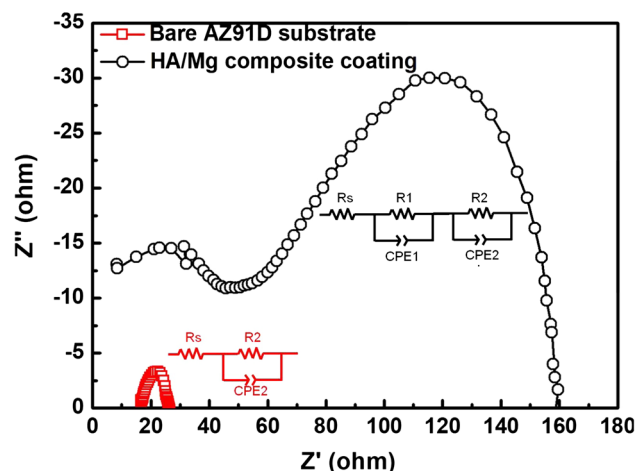

Fig. 5 Potentiodynamic polarization curves for HA/Mg coating and bare AZ91D substrate

Fig. 6 EIS and equivalent circuits for HA/Mg coating and bare AZ91D substrate

Table 2 Polarization results for the HA/Mg coating and bare AZ91D substrate

Samples	I_{corr}, $\mu A/cm^2$	E_{corr}, V	Corrosion rate, MPY	R_p, Ohms/cm^2
HA/Mg composite coating	81.8 ± 15.2	-1.482 ± 0.007	37.4 ± 7.7	331.9 ± 65.9
Bare AZ91D substrate	570.5 ± 79.5	-1.215 ± 0.012	264.2 ± 56.9	45.7 ± 12.5

Table 3 EIS results for the HA/Mg coating and bare AZ91D substrate

Sample	Rs, Ωcm^2	R1, Ωcm^2	CPE1, μFcm^{-2}	n1	R2, Ωcm^2	CPE2, $mFcm^{-2}$	n2
HA/Mg composite coating	2.81 ± 0.07	35.06 ± 4.4	2.79 ± 0.6	0.93 ± 0.01	151.6 ± 25.6	0.69 ± 0.01	0.39 ± 0.01
Bare AZ91D substrate	15.57 ± 2.26	…	…	…	6.53 ± 3.11	0.18 ± 0.1	0.79 ± 0.07
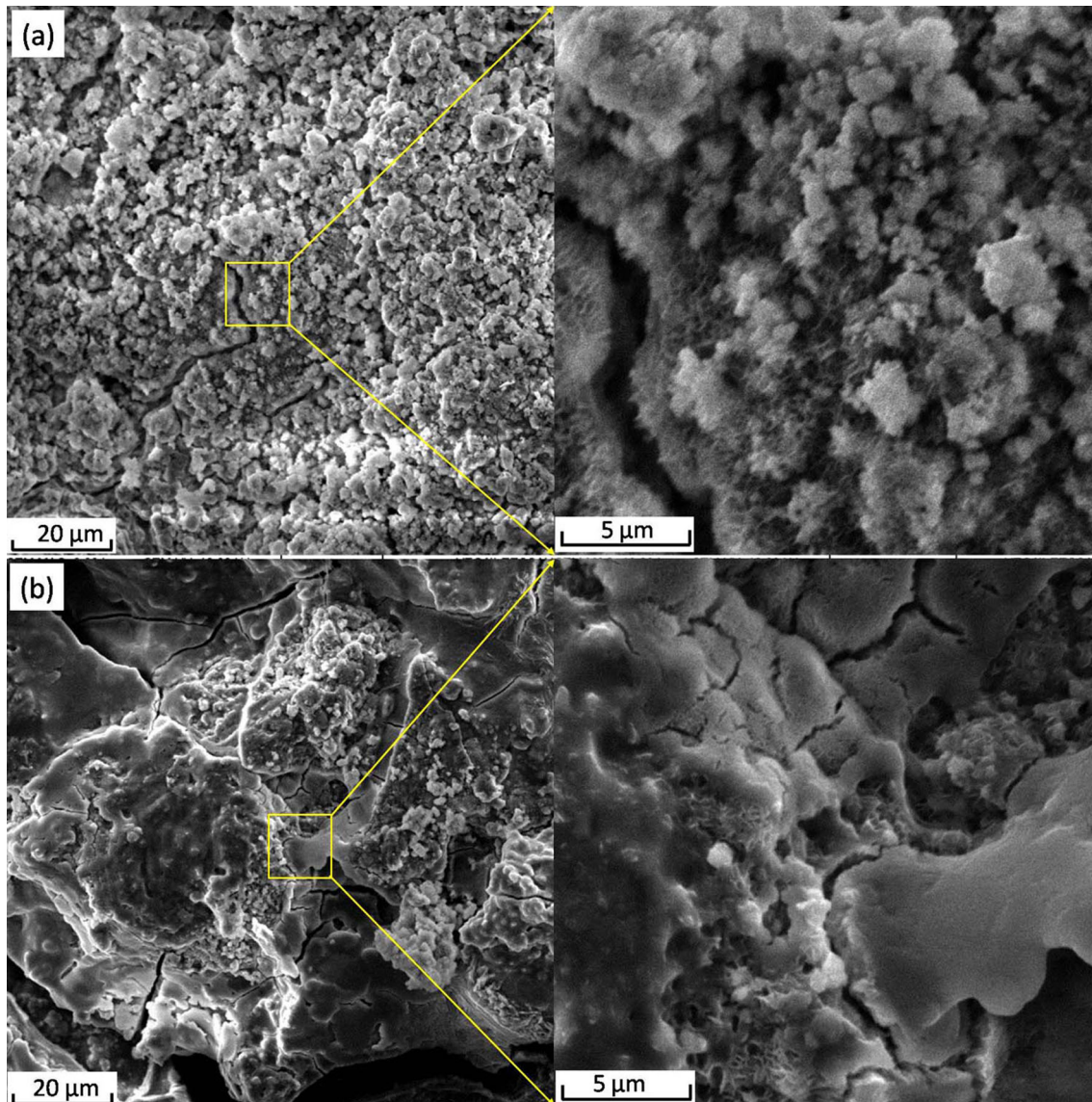
Fig. 7 Surface morphologies of both the HA/Mg composite coating (a) and bare AZ91D substrate (b) after the polarization tests

of Mg metal in HBSS during the polarization test (Ref 13). In contrast, on the surface of sand-blasted AZ91D after the polarization tests, there appeared some microcracks and smooth precipitation. The abrasive feature caused by sand-blasted disappeared (see Fig. 7b) indicating the dissolution of AZ91D substrate. To identify the formation of precipitations, the XRD analysis was performed on the surface of HA/Mg composite coating and bare AZ91D substrate after

the polarization tests (see Fig. 8). It is shown there existed $Mg(OH)_2$ peaks in the XRD pattern analyzed on these two surfaces and the relative intensities of Mg peaks decrease. It also shows the disappearance of MgO phase and the formation of $Mg(OH)_2$ phase (Ref 15). The $Mg(OH)_2$ phase is resulted from the chemical reaction as following (Ref 11, 33).
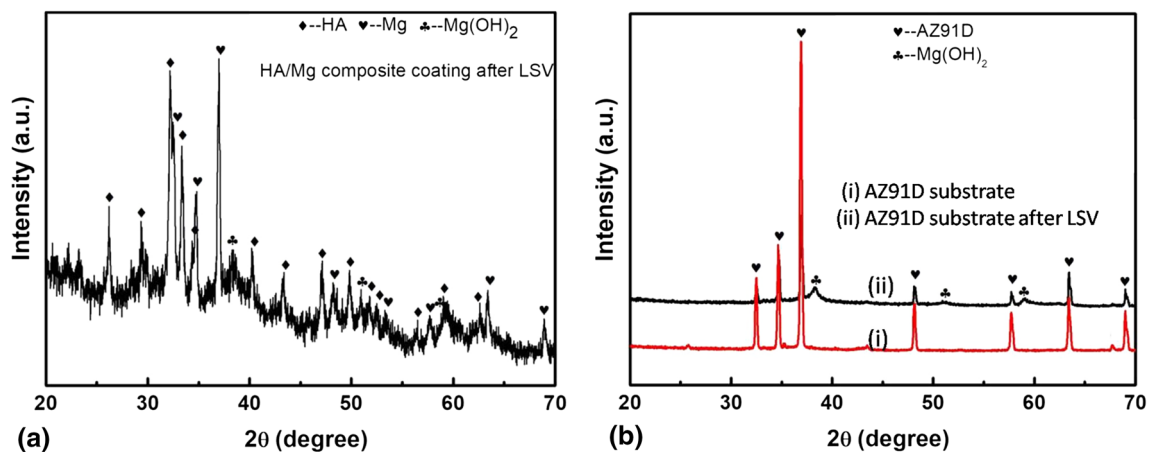
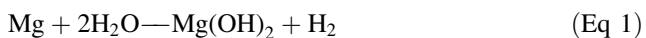**Fig. 8** XRD patterns of both the HA/Mg composite coating (a) and bare AZ91D substrate (b) after the polarization tests

$$Mg + 2H_2O \longrightarrow Mg(OH)_2 + H_2 \qquad (Eq\ 1)$$

$$MgO + H_2O \longrightarrow Mg(OH)_2 \qquad (Eq\ 2)$$

Usually, oxidization-formed MgO film on the surface of Mg was not compact, which cannot be a barrier layer on the Mg alloy substrate. However, it is reported that the cold-pressed MgO coating by using MgO nanoparticles on Mg alloy substrate can improve the corrosion resistance (Ref 11). The MAO film prepared by micro-arc oxidation method can also effectively hinder the corrosion medium diffusion through this kind of MAO film is porous (Ref 5). Evermore, addition of MgO to Mg/HA composite can increase its corrosion resistance compared to the Mg/HA composite (Ref 33). In the present study, although the oxidization-formed MgO film itself cannot hinder the corrosion medium penetration, it can decrease the mismatch of TEC between HA particles and Mg particles which would be liable to decrease the cracks between those heterogeneous particles in the HA/Mg composite coatings. Therefore, it can be considered that the MgO film is benefit to hinder the corrosion medium penetration. In addition, the HA splats in the composite coating can also hinder the corrosion medium diffusion by decreasing the Mg splat dissolution owing to its less solubility of HA than Mg (Ref 32, 33). Consequently, this HA/Mg composite coating can be a potential strategy to prepare biodegradable coatings on metal substrates for use in the implant field.

Conclusions

A HA/Mg composite coating was deposited onto AZ91D alloy by HVSFS. Both the Mg and HA were largely preserved in the composite coating with a slight amount of MgO. The HA/Mg composite coating exhibited a rough surface and a lamellar structure in the cross section as well as a well-bonded coating/substrate interface. The Mg particles showed superior deposition during the co-deposition of HA/Mg mixed powder. The HA/Mg composite coating significantly improved corrosion resistance performance of AZ91D substrate with a low corrosion current, corrosion rate and a high corrosion impedance. The composite coating and AZ91D substrate after polarization tests presented rough and cracked surfaces with the dissolution of Mg in HBSS. This HA/Mg composite coating can be a potential strategy to prepare biodegradable coatings on metal substrates for applications in the implant field.

References

1. R. Zeng, W. Dietzel, F. Witte, N. Hort, and C. Blawert, Progress and Challenge for Magnesium Alloys as Biomaterials, *Adv. Eng. Mater.*, 2010, **10**, p 12
2. S. Shadanbaz and G.J. Dias, Calcium Phosphate Coatings on Magnesium Alloys for Biomedical Applications: A Review, *Acta Biomater.*, 2012, **8**, p 20
3. M.S. Uddin, C. Hall, and P. Murphy, Surface Treatments for Controlling Corrosion Rate of Biodegradable Mg and Mg-Based Alloy Implants, *Sci. Technol. Adv. Mater.*, 2015, **16**, p 053501
4. D. Chen, R. Wang, Z. Huang, Y. Wu, Y. Zhang, and G. Wu, Evolution Processes of the Corrosion Behavior and Structural Characteristics of Plasma Electrolytic Oxidation Coatings on AZ31 Magnesium Alloy, *Appl. Surf. Sci.*, 2018, **434**, p 326
5. C. Wang, B. Jiang, M. Liu, and Y. Ge, Corrosion Characterization of Micro-arc Oxidation Composite Electrophoretic Coating on az31b Magnesium Alloy, *J. Alloy. Compd.*, 2015, **621**, p 53
6. W.F. Ng, M.H. Wong, and F.T. Cheng, Stearic Acid Coating on Magnesium for Enhancing Corrosion Resistance in Hanks' Solution, *Surf. Coat. Technol.*, 2010, **204**(11), p 1823

7. S. Gaur, R.K. Singh Raman, and A.S. Khanna, In Vitro Investigation of Biodegradable Polymeric Coating for Corrosion Resistance of mg-6zn-ca Alloy in Simulated Body Fluid, *Mater. Sci. Eng. C Mater. Biol. Appl.*, 2014, **42**, p 91

8. P. Amaravathy, S. Sowndarya, S. Sathyanarayanan, and N. Rajendran, Novel Sol Gel Coating of Nb_2O_5 on Magnesium Alloy for Biomedical Applications, *Surf. Coat. Technol.*, 2014, **244**(15), p 131

9. H. Amiri, I. Mohammadi, and A. Afshar, Electrophoretic Deposition of Nano-Zirconia Coating on AZ91D Magnesium Alloy for Bio-Corrosion Control Purposes, *Surf. Coat. Technol.*, 2016, **311**, p 182

10. F.M. Rojaee, K. Raeissi, and A. Sharifnabi, Biodegradation Assessment of Nanostructured Fluoridated Hydroxyapatite Coatings on Biomedical Grade Magnesium Alloy, *Ceram. Int.*, 2014, **40**, p 10

11. S.Z. Khalajabadi, A.H. Abu, N. Ahmad, M. Kadir, and A. Ismail, Biodegradable $Mg/HA/TiO_2$ Nanocomposites Coated with MgO and Si/MgO for Orthopedic Applications: A Study on the Corrosion, Surface Characterization and Biocompatability, *Coatings*, 2017, **7**, p 154

12. A. Arifin, A. Sulong, N. Muhamad, J. Syarif, and M.I. Ramli, Material Processing of Hydroxyapatite and Titanium Alloy (HA/Ti) Composite as Implant Materials Using Powder Metallurgy: A Review, *Mater. Des.*, 2014, **55**, p 165-175

13. M. Die, M.H. Kang, S.M. Kim, H.E. Kim, and J. Song, Hydroxyapatite (HA) Poly-L-Lactic Acid (PLLA) Dual Coating on Magnesium Alloy Under Deformation for Biomedical Applications, *J. Mater. Sci. Mater. Med.*, 2015, **27**, p 34

14. W. Fan, H. Du, Y. An, C. Guo, Y. Wei, and L. Hou, Fabrication and Characterization of a Hydroxyapatite–Methylcellulose Composite Coating on the Surface of AZ31 Magnesium Alloy, *Mater. Lett.*, 2015, **152**, p 32

15. S.Z. Khalajabadi, M.R.A. Kadir, S. Izman, H.R. Bakhsheshi-Rad, and S. Farahany, Effect of Mechanical Alloying on the Phase Evolution, Microstructure and Bio-Corrosion Properties of a $Mg/HA/TiO_2/MgO$ Nanocomposite, *Ceram. Int.*, 2014, **40**, p 17

16. M. Zhang, S. Cai, F.Y. Zhang, G.H. Xu, F.W. Wang, N. Yu, and X.D. Wu, Preparation and Corrosion Resistance of Magnesium Phytic Acid/Hydroxyapatite Composite Coatings on Biodegradable AZ31 Magnesium Alloy, *J. Mater. Sci. Mater. Med.*, 2017, **28**, p 82

17. G.Y. Xiong, Y.J. Nie, D.H. Ji, J. Li, C.Z. Li, W. Li, Y. Zhu, H.L. Luo, and Y.Z. Wan, Characterization of Biomedical Hydroxyapatite/Magnesium Composites Prepared by Powder Metallurgy Assisted with Microwave Sintering, *Curr. Appl. Phys.*, 2016, **16**, p 830

18. J. Kubasek, D. Vojtech, J. Maixner, and D. Dvorsky, The Effect of Hydroxyapatite Reinforcement and Preparation Methods on the Structure and Mechanical Properties of Mg-HA Composites, *Sci. Eng. Compos. Mater.*, 2017, **24**, p 297

19. X.Y. Ni, A.J. Li, X.B. Xiong, R.C. Bai, and D. Zhou, Effect of Electromagnetic Induction Deposition's Heating Time of Magnesium-Hydroxyapatite Coating on Carbon/Carbon Composites, *J. Biobased Mater. Bioener.*, 2014, **8**, p 603

20. C.C. Berndt, M.F. Hasan, U. Tietz, and K.P. Schmitz, A Review of Hydroxyapatite Coatings Manufactured by Thermal Spray, vol. 2, p. 267. Springer, Berlin (2014)

21. H.L. Yao, H.T. Wang, X.B. Bai, G.C. Ji, and Q.Y. Chen, Improvement in Mechanical Properties of Nano-Structured HA/TiO_2 Multilayer Coatings Deposited by High Velocity Suspension Flame Spraying (HVSFS), *Surf. Coat. Technol.*, 2018, **342**, p 94

22. H.L. Yao, Y.L. Zou, X.B. Bai, H.T. Wang, G.C. Ji, and Q.Y. Chen, Microstructures, Mechanical Properties and Electrochemical Behaviors of Nano-structured HA/Ti Composite Coatings Deposited by High-Velocity Suspension Flame Spray (HVSFS), *Ceram. Int.*, 2018, **44**, p 13024

23. M.E. Derevyaga, Effect of Pressure on Magnesium Combustion, *Combust. Explos. Shock Waves*, 1983, **19**, p 31

24. H.M. Cassel and I. Liebman, Combustion of Magnesium Particles I, *Combust. Flame*, 1962, **6**, p 153

25. Y. Lu, M. Li, S. Li, Z. Wang, and R. Zhu, Plasma-Sprayed Hydroxyapatite + Titania Composite Bond Coat for Hydroxyapatite Coating on Titanium Substrate, *Biomaterials*, 2004, **25**(18), p 4393

26. M.H. Song, G.H. Wu, G.Q. Chen, and W.S. Yang, Thermal Expansion and Dimensional Stability of Unidirectional and Orthogonal Fabric M40/AZ91D Composites, *Trans. Nonferrous Metals Soc. China*, 2010, **20**(1), p 47

27. R.B. Heimann, Plasma-Sprayed Hydroxylapatite Coatings as Biocompatible Intermediaries Between Inorganic Implant Surfaces and Living Tissue, *J. Therm. Spray Technol.* **1** (2018).

28. Y.F. Ding, C.E. Wen, P. Hodgson, and Y.C. Li, Effects of Alloying Elements on the Corrosion Behavior and Biocompatibility of Biodegradable Magnesium Alloys: A Review, *J. Mater. Chem. B*, 2014, **2**, p 1912

29. R.D. Campo, B. Savoini, A. Muñoz, M.A. Monge, and G. Garcés, Mechanical Properties and Corrosion Behavior of Mg-HAp Composites, *J. Mech. Behav. Biomed. Mater.*, 2014, **39**, p 238

30. F. Witte, F. Feyerabend, P. Maier, J. Fischer, M. Störmer, and C. Blawert, Biodegradable Magnesium-Hydroxyapatite Metal Matrix Composites, *Biomaterials*, 2007, **28**(13), p 2163

31. K. Mensah-Darkwa, R.K. Gupta, and D. Kumar, Mechanical and Corrosion Properties of Magnesium–Hydroxyapatite (Mg–HA) Composite Thin Films, *J. Mater. Sci. Technol.*, 2013, **29**(9), p 788

32. Y.L. Gao, Y. Liu, and X.Y. Song, Plasma-Sprayed Hydroxyapatite Coating for Improved Corrosion Resistance and Bioactivity of Magnesium Alloy, *J. Therm. Spray Technol.*, 2018, https://doi.org/10.1007/s11666-018-0760-9

33. S.Z. Khalajabadi, M.R.A. Kadir, S. Izman, and M. Marvibaigi, The Effect of Mgo on the Biodegradation, Physical Properties and Biocompatibility of a Mg/HA/MgO Nanocomposite Manufactured by Powder Metallurgy Method, *J. Alloy. Compd.*, 2016, **655**, p 266